International Journal of the Physical Sciences Vol. 6(30), pp. 6995 - 7006, 23 November, 2011
Available online at http://www.academicjournals.org/IJPS
DOI: 10.5897/IJPS11.921
ISSN 1992 - 1950 ©2011 Academic Journals

Full Length Research Paper

An object-oriented approach of generic diffusion computing for three dimensional ultrasound volumetric images

Lai Khin Wee[1,2]*, Hum Yan Chai[2] and Eko Supriyanto[2]

[1]Biomedical Engineering Department, Faculty of Computer Science and Automation, Institute of Biomedical Engineering and Informatics, Technische Universität Ilmenau, 98684, Ilmenau, Thuringia, Germany.
[2]Department of Clinical Science and Engineering, Faculty of Health Science and Biomedical Engineering, Universiti Teknologi Malaysia, 81310 Skudai, Johor, Malaysia.

Accepted 20 October, 2011

Medical image information representation using two dimensional image planes have major drawbacks on the grounds that the there are technical constrains in providing the optimized spatial orientation and physical limitations. In comparison, three dimensional imaging shows higher degree of versatility in clinical application. Conventional anisotropic diffusion and speckle removal might have promising performance on 2D ultrasonic images, but it is not effective in 3D ultrasonic images. In this paper, we have developed extension algorithms for 3D diffusion in ultrasonic volume rendering using open source visualization toolkits. Investigations have been conducted on 3D volume rendering based on visualization toolkit (VTK) generic computing and the simulation results were compared with ordinary 2D diffusion in 3D ultrasonic image. Obstructive effect was eliminated with the proposed technique by conserving information between neighboring 2D slices. The experimental results show the significant improvement of 3D diffusion on 3D ultrasound volume rendering.

Key words: Three dimensional, ultrasound, volume, diffusion, rendering, visualization toolkit (VTK), open sources.

INTRODUCTION

Ultrasound medical imaging is widely used nowadays in clinical application due to its intuitive, convenient, safety, non-invasive, and low cost (Catherine and Tal, 2010; Min and Myoung, 2007; Wee at al., 2010; Wee and Supriyanto, 2010; Wee et al., 2011a, b, c; Yu et al., 2007). Nevertheless, the restrictions on the imaging mechanism lead to low resolution in ultrasound images and they have always been a major drawback in its imaging modality. This condition will be more complicated when the subjects of interest are the inhomogeneity fine structure of organ or tissue. Some minor structures cannot be resolved by ultrasound formation, and when it is coupled with the interference of acoustic signals, the ultrasound images form a well-known unique spot, namely speckle noise. Obviously, it will greatly reduce the ultrasound image quality, and make the identification and analysis of image detail become more challenging. Therefore, it is necessary to perform de-noising.

The current popular filters for ultrasonic images includes median-based filtering (Czerwinski et al., 1995), homomorphic filtering (Christos and Constantinos, 2011; Rajeev and Gupta, 2010; Gupta et al., 2005), wavelet transform (Kashif et al., 2008; Shirzad et al., 2009; Gupta et al., 2003) and anisotropic diffusion (Christos et al., 2006; Deepti et al., 2010; Ling et al., 2007; Paula et al., 2009). Based on previous examination, median-based filtering technique refers to the local image noise's statistical characteristics in order to select the filtering window's size and shape automatically. Nevertheless, these methods are very sensitive in choosing the

*Corresponding author. E-mail: kwlai2@live.utm.my, khin-wee.lai@tu-ilmenau.de. Tel: +4915774853251. Fax: +493677691311.

shape and size of the window; even the adaptive window size is still limited in its filtering effect. Homomorphic filtering method is based on the image logarithmic transformation; the multiplicative noise is turned into additive noise and filtered by conventional methods. Wavelet transform filtering method converts the ultrasound images in wavelet domain in order to discard some of the elements size, and it is followed by inverse transform to remove undesired noise. However, this method confront with difficulty in choosing the right element size, if the discarded signal are over small-scale, it fails to remove the noise effectively or vice versa, it may lose useful signal in large-scale signals removal.

In recent years, filtering method based on the diffusion equation emerges as a popular filtering technique for ultrasound medical image. It is based on the principal in solving the initial value of input image using nonlinear heat diffusion equation. Perona and Malik (1990) initiate the proposed anisotropic diffusion equation (referred as P-M model) for image denoising. The extreme advantage of their proposed techniques is having great protection on image edges, while smoothing and denoising the image features without distortion. Their diffusion model has aroused great interest among the researcher worldwide in the last ten years, causing a boom on partial differential equation enhancement in image processing. By introducing image features, diffusion equations are designed to control the appropriate spread of the diffusion coefficient, producing the smooth image and enhancing the image feature information simultaneously.

However, the direct practicing of P-M model on medical ultrasonic image is not satisfactory. The inefficiency of P-M model is predicated on its inherent incapability in solving the additive noise. For ultrasonic images with additive noise, P-M model (Perona and Malik, 1990) shows promising de-noising effect. Nevertheless, the resulting outcome of P-M model on multiplicative noise in ultrasound image shows very limited effect, sometimes even counterproductive. Over a decade of research and exploration on anisotropic diffusion enhancement, it is now a powerful speckle noise removal called SRAD for 2D ultrasound images (Yu and Acton, 2002). Much of the research attentions are focus on 2D diffusion implementtation, rather than 3D ultrasound images. Theoretically, conventional 2D SRAD diffusion equations are also able to diffuse in 3D ultrasound images by performing diffusion on each slice of collective 2D images before reconstructing them into 3D model. Nonetheless, these render an obstructive effect in space direction of the 3D model in response to the missing information between slices of 2D image.

In this paper, we have extended the generic computing of anisotropic diffusion on 3D ultrasound volume images in VTK open source computing approach. In the present research, we have investigated the effect of 2D diffusion on a serial of 2D ultrasound images, before further reconstructing them into 3D volume rendering. Follow by that, we have compared this result with the implementtation of direct 3D diffusion on volume images. For analyzing reason, we have also displayed the original 3D volume rendering without diffusion, and this proves the significant contribution of proposed method.

PREVIOUS WORK AND REVIEW

Principle and implementation of anisotropic diffusion

The earliest diffusion technique was proposed by Lee in 1980 (Lee, 1980); Lee's filter suggested that additive noises are approximately similar as a linear model based on MMSE principle. Even though Lee's filter is equipped with diffusion features, it remains a window-based filtering method, where it applies the same diffusion coefficient in all spreading direction, and this is inextricably linked to weak image features preservation and the aftermath: Blurred boundaries.

In 1990, Perona and Malik (Perona and Malik, 1990) proposed an advancement technique in order to maintain the edge of image features, namely anisotropic diffusion, which depends on the image gradient in various spreading direction to determine diffusion coefficient. P-M model has increased the performance in smoothing noise while retaining image details without distorting edge of image boundaries. A decade later, limitations of P-M model as described by Yu and Acton (2002) have been improved to SRAD which is equipped with the edge localization capability and mean preservation.

The anisotropic diffusion of P-M model is as follow;

$$\frac{\partial I}{\partial t} = div\left(c(x,y,t)\nabla I\right) = \nabla c \cdot \nabla I + c(x,y,t)\Delta I \quad (1)$$

With the condition,

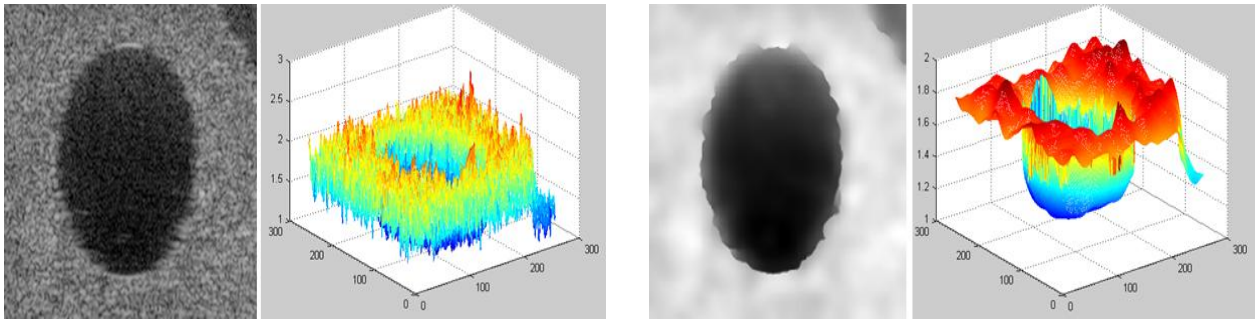
$$I(t=0) \equiv I_0$$

where ∇ denotes the gradient operator, *div*, the divergence operator, *c(x, y)*, the diffusion coefficient, *t*, the diffusion time, Δ, Laplacian of *I*, and I_0 the initial image. *C (t)* controls the rate of diffusion and is usually chosen as a function of the image gradient so as to preserve edges in the image.

Two forms of Perona and Malik proposed C (model) are;

$$c\left(\left|\nabla I\right|\right) = \exp\left[-\left(\frac{\left|\nabla I\right|}{k}\right)^2\right] \quad (2)$$

$$c\left(\left|\nabla I\right|\right) = \frac{1}{1+\left(\left|\nabla I\right| / k\right)^2} \quad (3)$$



(a) (b)

Figure 1. Diffusion based on number of iteration; (a) diffusion iteration = 1, and (b) diffusion iteration = 200.

where *k* denotes the edge magnitude factor, correlated to the contradiction degree's balance of edge preservation and smoothing factor, and final smoothing outcomes are influenced by diffusion time *t*. The basic idea of P-M model is using $c(\|\nabla I\|)$ to control the diffuse proliferation on the initial image. The model achieving adaptive diffusion is based on image gradient magnitude. At the edges with large gradient modulus, $c(\|\nabla I\|)$ whichever is less; the model is weak in smooth implementation to protect the edge information. In the homogenous areas, gradient modulus is smaller, $c(\|\nabla I\|)$ become larger; the model has more smoothing effect. Adaptive selection of smoothing degree at the edge and homogeneous region can help to identify the boundary location, and solved the contradiction between de-noising and edge retention.

Enhanced speckle reduction anisotropic diffusion

Due to the limitation of P-M model, a robust diffusion method is suggested by Yu and Acton (2002) which comprises a strong edge preserving filter and this makes it to have an edge over the conventional speckle removal filters. The proposed SRAD exploits the instantaneous coefficient of variation (ICOV), which is shown to be a function of the local gradient magnitude and Laplacian operators. The diffusion coefficient in 2D SRAD is a function of *q*, where *q(x, y; t)* are shown as follows;

$$c(x,y;t)=\frac{1}{1+\frac{\left[q^2(x,y;t)-q_0^2(t)\right]}{q_0^2(t)\left(1+q_0^2(t)\right)}} \quad (4)$$

$$q(x,y;t)=\sqrt{\frac{\left(\frac{1}{2}\right)\left(\frac{|\nabla I|}{I}\right)^2-\left(\frac{1}{4^2}\right)\left(\frac{\nabla^2 I}{I}\right)^2}{\left[1+\left(\frac{1}{4}\right)\left(\frac{\nabla^2 I}{I}\right)\right]^2}} \quad (5)$$

And the initial speckle scale computed homogenous region q_0 is shown as follows;

$$q_0(t)=\frac{\sqrt{\mathrm{var}\left[z(t)\right]}}{\overline{z(t)}} \quad (6)$$

where *I* denotes input image, ∇, gradient operator, and |, the magnitude. The function shows high value at edge and low value in homogenous region. Moreover, the diffusion order can be revealed from our simulations in Figure 1 which demonstrates that ICOV successfully smoothen the speckled region and intensifies the contrast between constructive object and noise area.

Value of diffusion coefficient is influenced by ICOV where edge pixel area activates a lower diffusion coefficient and indirectly decreases the level of diffusion. Speckle area produces higher value of diffusion coefficient which increases the smoothing effect in certain area. Figure 2 illustrates the smoothing of ultrasound image with difference number of iteration and smoothing time step.

Ultrasound image changes gradually in every iteration. Larger iteration will generate a smoother image but it requires longer processing period and over-smoothing may destroy the edge of ultrasound image. Figure 3 shows our simulation results on ultrasound phantom with appropriate diffusion iteration.

METHODS

As 3D models and visualization are getting widely implemented in scientific computing applications and intense development of object-oriented programming, there is a need to have a simple, object-oriented features and easy-to-transplant 3D graphics to realize the 3D diffusion algorithms on 3D ultrasound volume rendering.

For instance, the most straight forward method to diffuse 3D ultrasonic model is performing 2D SRAD on each of the collective 2D slices before they are further reconstructed into 3D volume rendering. Nevertheless, this simple method will result in an

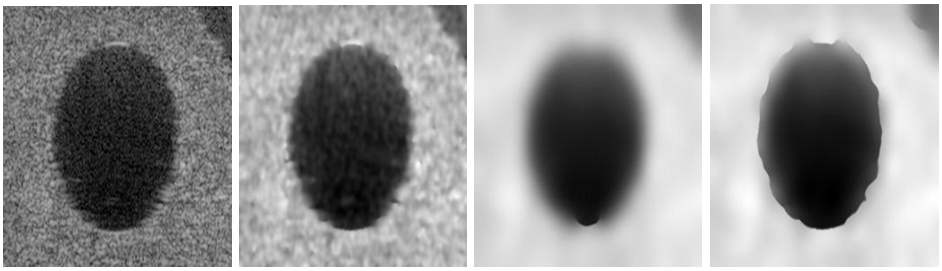


Figure 2. Level of smoothing (a) original ultrasonic image (b) under-smoothing (c) over-smoothing (d) smoothing at appropriate iteration.

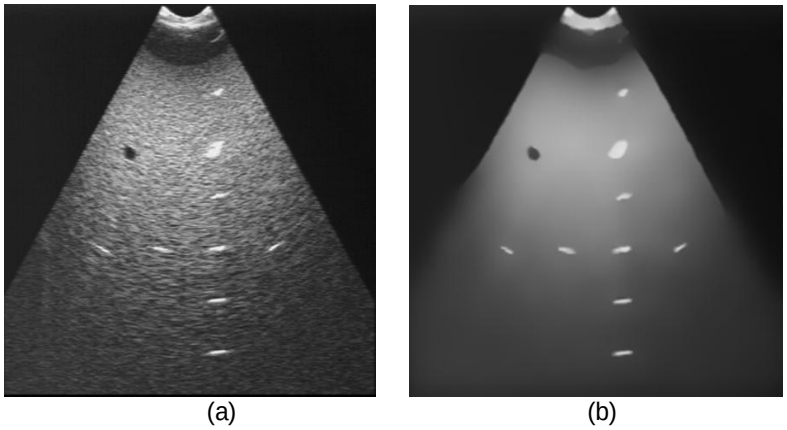


Figure 3. Simulation results comparison (a) before 2D SRAD, and (b) after 2D SRAD.

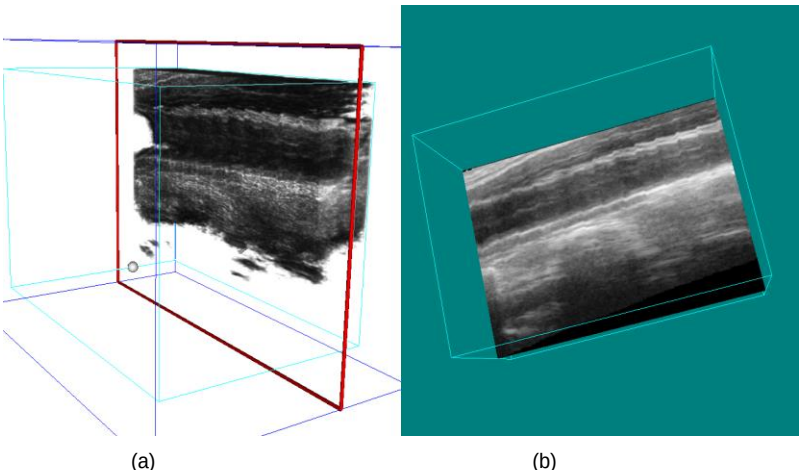


Figure 4. Simulation results in 3D ultrasound volume (a) XZ view on 3D visualization, and (b) 2D re-slice of viewed XZ plane.

obstructive effect in 3D volume, especially in Z-pixels direction due to the missing information in spacing track. Image features in between neighboring slices were not conserved during implementation of 2D SRAD. In our investigation, we have simulated this limitation on a series of 2D ultrasound images collected on a volunteer's carotid artery as shown in Figure 4.

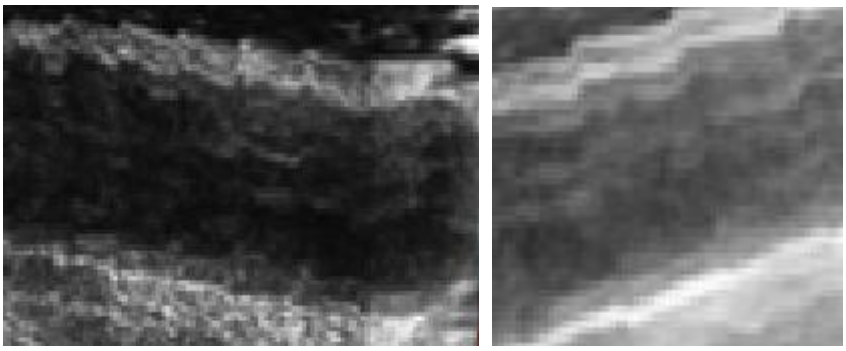


Figure 5. Obstructive line effect (a) on 3D volume rendering, and (b) on 2D ultrasonic slices.

Close observation on Figure 4 shows that obstructive effects are present in spacing direction, as shown in Figure 5. Measurement on XY direction will not encounter with this limitation, but this effect will cause wrong measurement especially when the subjects of interest are in small scale. Important morphology was destroying when we visualize in 3D volume mode.

3D Diffusion algorithm designs

3D diffusion algorithms are developed in the present studies. It will operate directly on 3D volumetric images rather than every 2D slices. Thus, information between slices of 2D image are explored and preserved.

By following Equation 1 to 3, the subsequent shows the existing 2D anisotropic diffusion equations and its derivation in 2D discrete implementation. We have expanded the diffusion to spread in eight directions, which includes the east, west, north, south, and east-north, west-north, east-south and west-south pixel $f(x,y)$ direction.

$$\frac{\partial}{\partial t}I(x,y,t) = div[g(x,y,t) * \nabla I(x,y,t)]$$
$$= \frac{\partial}{\partial x}\left[g(x,y,t) * \frac{\partial}{\partial x}I(x,y,t)\right] + \frac{\partial}{\partial y}\left[g(x,y,t) * \frac{\partial}{\partial y}I(x,y,t)\right]$$

$$= \frac{1}{(\Delta x)^2}\left[g\left(x+\frac{\Delta x}{2}, y, t\right) * (I(x+\Delta x, y, t) - I(x,y,t)) + g\left(x-\frac{\Delta x}{2}, y, t\right) * (I(x-\Delta x, y, t) - I(x,y,t))\right]$$
$$+ \frac{1}{(\Delta y)^2}\left[g\left(x, y+\frac{\Delta y}{2}, t\right) * (I(x, y+\Delta y, t) - I(x,y,t)) + g\left(x, y-\frac{\Delta y}{2}, t\right) * (I(x, y-\Delta y, t) - I(x,y,t))\right]$$
$$+ \frac{1}{(\Delta d)^2}\left[g\left(x+\frac{\Delta x}{2}, y+\frac{\Delta y}{2}, t\right) * (I(x+\Delta x, y+\Delta y, t) - I(x,y,t)) + g\left(x-\frac{\Delta x}{2}, y-\frac{\Delta y}{2}, t\right) * (I(x-\Delta x, y-\Delta y, t)\right.$$
$$\left. - I(x,y,t))\right] + \frac{1}{(\Delta d)^2}\left[g\left(x+\frac{\Delta x}{2}, y-\frac{\Delta y}{2}, t\right) * (I(x+\Delta x, y-\Delta y, t) - I(x,y,t))\right.$$
$$\left. + g\left(x-\frac{\Delta x}{2}, y+\frac{\Delta y}{2}, t\right) * (I(x-\Delta x, y+\Delta y) - I(x,y,t))\right]$$
$$= \phi_{east} + \phi_{west} + \phi_{north} + \phi_{south} + \phi_{eastnorth} + \phi_{westnorth} + \phi_{eastsouth} + \phi_{westsouth} \quad (7)$$

For relative distance, $\Delta x = \Delta y = 1$, $\Delta d = \sqrt{2}$

The anisotropic diffusion filtering entails iterative update on each pixel in the image by the flow intensity contributed by its eight neighboring pixels:

$$\frac{\partial}{\partial t}I(x,y,t+\Delta t) \approx I(x,y,t) + \Delta t\left[\phi_{east} + \phi_{west} + \phi_{north} + \phi_{south} + \frac{1}{(\Delta d)^2}(\phi_{eastnorth} + \phi_{westnorth} + \phi_{eastsouth} + \phi_{westsouth})\right]$$
$$= I(x,y,t) + \Delta t\left[\phi_{east} + \phi_{west} + \phi_{north} + \phi_{south} + \frac{1}{2}(\phi_{eastnorth} + \phi_{westnorth} + \phi_{eastsouth} + \phi_{westsouth})\right] \quad (8)$$

For 3D diffusion algorithm designs, we have extended Equations (7) and (8) to three dimensional discrete form. The 3D discrete implementation of anisotropic diffusion in 26 directions is derived as following:

$$\frac{\partial}{\partial t}I(x,y,z,t) = div[g(x,y,z,t) * \nabla I(x,y,z,t)]$$
$$= \frac{\partial}{\partial x}[g(x,y,,zt) * \frac{\partial}{\partial x}I(x,y,z,t)] + \frac{\partial}{\partial y}[g(x,y,,z,t) \bullet \frac{\partial}{\partial y}I(x,y,z,t)]$$

$$+ \frac{\partial}{\partial z}[g(x,y,z,t) \bullet \frac{\partial}{\partial z}I(x,y,z,t)]$$
$$= \frac{1}{(\Delta x)^2}[g(x+\frac{\Delta x}{2}), y, z, t) \bullet (I(x+\Delta x, y, z, t) - I(x,y,z,t))$$
$$+ g(x-\frac{\Delta x}{2}, y, z, t) \bullet (I(x-\Delta x, y, z, t) - I(x,y,z,t))]$$
$$+ \frac{1}{(\Delta y)^2}[g(x, y+\frac{\Delta y}{2}, zt) \bullet (I(x, y+\frac{\Delta y}{2}, z, t) - I(x,y,t))$$
$$+ g(x, y-\frac{\Delta y}{2}, z, t) \bullet (I(x, y-\Delta y, z, t) - I(x,y,z,t))]$$
$$+ \frac{1}{(\Delta z)^2}[g(x, y, z+\frac{\Delta z}{2} t) \bullet (I(x, y, z+\frac{\Delta z}{2}, t) - I(x,y,t))$$
$$+ g(x, y, z-\frac{\Delta z}{2}, t) \bullet (I(x, y, z-\Delta z, t) - I(x,y,z,t))]$$
$$+ \frac{1}{(\Delta d_1)^2}[g(x-\frac{\Delta x}{2}, y-\frac{\Delta y}{2}, z, t) \bullet (I(x-\Delta x, y-\Delta y, z, t) - I(x,y,t))$$
$$+ g(x+\frac{\Delta x}{2}, y+\frac{\Delta y}{2}, z, t) \bullet (I(x+\Delta x, y+\Delta y, z, t) - I(x,y,z,t))]$$
$$+ \frac{1}{(\Delta d_1)^2}[g(x-\frac{\Delta x}{2}, y+\frac{\Delta y}{2}, z, t) \bullet (I(x-\Delta x, y-\Delta y, z, t) - I(x,y,z,t))$$
$$+ g(x+\frac{\Delta x}{2}, y-\frac{\Delta y}{2}, z, t) \bullet (I(x+\Delta x, y-\Delta y, z, t) - I(x,y,z,t))]$$

$$+ \frac{1}{(\Delta d_2)^2}[g(x+\frac{\Delta x}{2}, y+\frac{\Delta y}{2}, z+\frac{\Delta z}{2}, t) \bullet (I(x+\Delta x, y+\Delta y, z+\Delta z, t) - I(x,y,z,t))$$
$$+ g(x-\frac{\Delta x}{2}, y-\frac{\Delta y}{2}, z-\frac{\Delta z}{2}, t) \bullet (I(x-\Delta x, y-\Delta y, z-\Delta z) - I(x,y,z,t))]$$
$$+ \frac{1}{(\Delta d_2)^2}[g(x+\frac{\Delta x}{2}, y+\frac{\Delta y}{2}, z-\frac{\Delta z}{2}, t)] \bullet (I(x+\Delta x, y+\Delta y, z-\Delta z, t) - I(x,y,z,t))$$
$$+ g(x-\frac{\Delta x}{2}, y-\frac{\Delta y}{2}, z+\frac{\Delta z}{2}, t) \bullet (I(x-\Delta x, y-\Delta y, z+\Delta z, t) - I(x,y,z,t))]$$
$$+ \frac{1}{(\Delta d_2)^2}[g(x+\frac{\Delta x}{2}, y-\frac{\Delta y}{2}, z+\frac{\Delta z}{2}, t) \bullet (I(x+\Delta x, y-\Delta y, z+\Delta z, t) - I(x,y,z,t)$$
$$+ g(x-\frac{\Delta x}{2}, y+\frac{\Delta y}{2}, z-\frac{\Delta z}{2}, t) \bullet (I(x-\Delta x, y+\Delta y, z-\Delta z, t) - I(x,y,z,t)]$$
$$+ \frac{1}{(\Delta d_2)^2}[g(x-\frac{\Delta x}{2}, y+\frac{\Delta y}{2}, z+\frac{\Delta z}{2}, t) \bullet (I(x-\Delta x, y+\Delta y, z+\Delta z, t) - I(x,y,z,t))$$
$$+ g(x+\frac{\Delta x}{2}, y-\frac{\Delta y}{2}, z-\frac{\Delta z}{2}, t) \bullet (I(x+\Delta x, y-\Delta y, z-\Delta z, y) - I(x,y,z,t))]$$
$$+ \frac{1}{(\Delta d_3)^2}[g(x-\frac{\Delta x}{2}, y, z+\frac{\Delta z}{2}, t) \bullet (I(x+\Delta x, y, z+\Delta z, t) - I(x,y,t))$$
$$+ g(x+\frac{\Delta x}{2}, y, z+\frac{\Delta z}{2}, t) \bullet (I(x+\Delta x, y, z+\Delta z, t) - I(x,y,z,t))]$$
$$+ \frac{1}{(\Delta d_3)^2}[g(x, y-\frac{\Delta y}{2}, z+\frac{\Delta z}{2}, t) \bullet (I(x, y-\Delta y, z+\Delta z, t) - I(x,y,z,t))$$
$$+ g(x, y+\frac{\Delta y}{2}, z+\frac{\Delta z}{2}, y) \bullet (I(x, y+\Delta y, z+\Delta z, t) - I(x,y,z,y))]$$

$$+ \frac{1}{(\Delta d_3)^2}[g(x-\frac{\Delta x}{2}, y, z-\frac{\Delta z}{2}, t) \bullet (I(x+\Delta x, y, z-\Delta z, t) - I(x,y,t))$$
$$+ g(x+\frac{\Delta x}{2}, y, z-\frac{\Delta z}{2}, t) \bullet (I(x+\Delta x, y, z-\Delta z, t) - I(x,y,z,t))]$$
$$+ \frac{1}{(\Delta d_3)^2}[g(x, y-\frac{\Delta y}{2}, z-\frac{\Delta z}{2}, t) \bullet (I(x, y-\Delta y, z-\Delta z, t) - I(x,y,z,t))$$
$$+ g(x, y+\frac{\Delta y}{2}, z-\frac{\Delta z}{2}, y) \bullet (I(x, y+\Delta y, z-\Delta z, t) - I(x,y,z,y))]$$

$$= \Phi_{east}(\Delta x) + \Phi_{west}(\Delta x) + \Phi_{north}(\Delta y) + \Phi_{south}(\Delta y) + \Phi_{up}(\Delta z) + \Phi_{down}(\Delta z) \quad (9)$$

where Δx, Δy, Δz, $\Delta d_1, \Delta d_2, \Delta d_3$ are relative distances between $I(x,y,z,t)$ and its nearest neighbours in the 26 directions respectively.

Determination of $\Delta x, \Delta y, \Delta z$, $\Delta d_1, \Delta d_2, \Delta d_3$ relative distance between neighbour and central node.

$$\Delta x = 1$$
$$\Delta y = 1$$
$$\Delta z = 1$$

$$\Delta d_1 = \sqrt{1^2 + 1^2} = \sqrt{2}$$
$$\Delta d_2 = \sqrt{\sqrt{(1^2 + 1^2)^2 + 1^2}} = \sqrt{3}$$
$$\Delta d_3 = \sqrt{1^2 + 1^2} = \sqrt{2}$$

The filtering process requires recursive operation on each pixel in the image by an amount relative to the flow contributed by its 26 nearest neighbors:

$$I(x,y,z,t+\Delta t) \approx I(x,y,z,t) + \Delta t \bullet [\Phi_{east}(\Delta x) + \Phi_{west}(\Delta x) + \Phi_{north}(\Delta y) + \Phi_{south}(\Delta y)$$
$$+ \Phi_{up}(\Delta z) + \Phi_{down}(\Delta z) + \Phi_{westnorth}(\Delta d_1) + \Phi_{eastsouth}(\Delta d_1) + \Phi_{westsouth}(\Delta d_1) + \Phi_{eastnorth}(\Delta d_1)$$
$$+ \Phi_{eastsouthup}(\Delta d_2) + \Phi_{westnorthdown}(\Delta d_2) + \Phi_{eastsouthdown}(\Delta d_2) + \Phi_{westnorthup}(\Delta d_2)$$
$$+ \Phi_{eastnorthup}(\Delta d_2) + \Phi_{westsouthdown}(\Delta d_2) + \Phi_{westsouthup}(\Delta d_2) + \Phi_{eastnorthdown}(\Delta d_2)$$
$$+ \Phi_{east,up}(\Delta d_3) + \Phi_{west,up}(\Delta d_{3)} + \Phi_{north,up}(\Delta d_3) + \Phi_{south,down}(\Delta d_3)$$
$$+ \Phi_{east,down}(\Delta d_3) + \Phi_{west,down}(\Delta d_3) + \Phi_{north,down}(\Delta d_3) + \Phi_{south,down}(\Delta d_3)] \quad (10)$$

Table 1. Determination of the upper bound.

Dimension	Neighbor	*N*
1	2	1/3
2	4	1/5
	8	1/7
3	6	1/7
	26	3/44

N for the discrete formulation of the diffusion process.

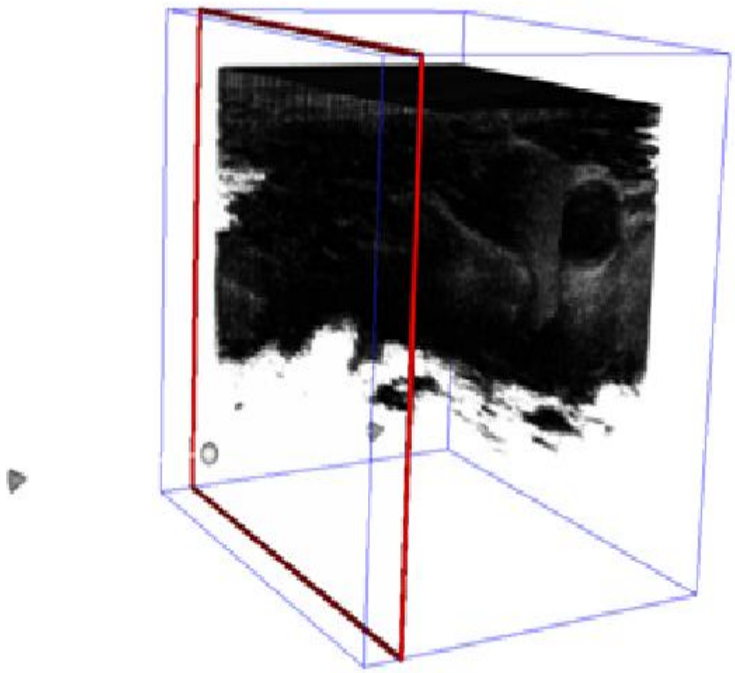


Figure 6. Original reconstruction 3D volume rendering without diffusion.

Determination of Δt

The upper bound, N can be determined from the discrete formulation of the diffusion process (spatial indices have been dropped for clarity). It is a numerical integration of a partial differential equation in order to perform the discrete implementation of the nonlinear anisotropic diffusion filtering. Gerig et al. (1992) has analyzed the filter and find bounds for the integration constant, Δt which must be in the range of zero and *N* where *N* is a positive real number as shown in Table 1.

The effect of Δt can viewed as an approximation for continuous case in integration for discrete implementation. The closer the value of Δt is to zero, the more accurate the approximation of discrete implementation compare to continuous case and vice versa.

Despite the high accuracy in approximation, the filter entails many iteration steps to yield good result.

RESULTS

In the proposed study, multi frames of DICOM ultrasound data were collected for 3D volume reconstructions. The collected DICOM files are stored in 8 bit depth, and digital unsigned characteristic with the grey scale value between 0 and 255. The maximum numbers of frames stored are 256 frames using Acuson Siemen ultrasound machine with spacing value at 3.57.

The order of these 256 ultrasound images need to be arranged according to their priority in advanced. The scanned subject in the present studies is carotid arteries, with the resolution 641 × 598 using trans-abdominal 3.5 MHz ultrasound transducer with freeze capability. Figure 6 shows the original restructured 3D ultrasound volume

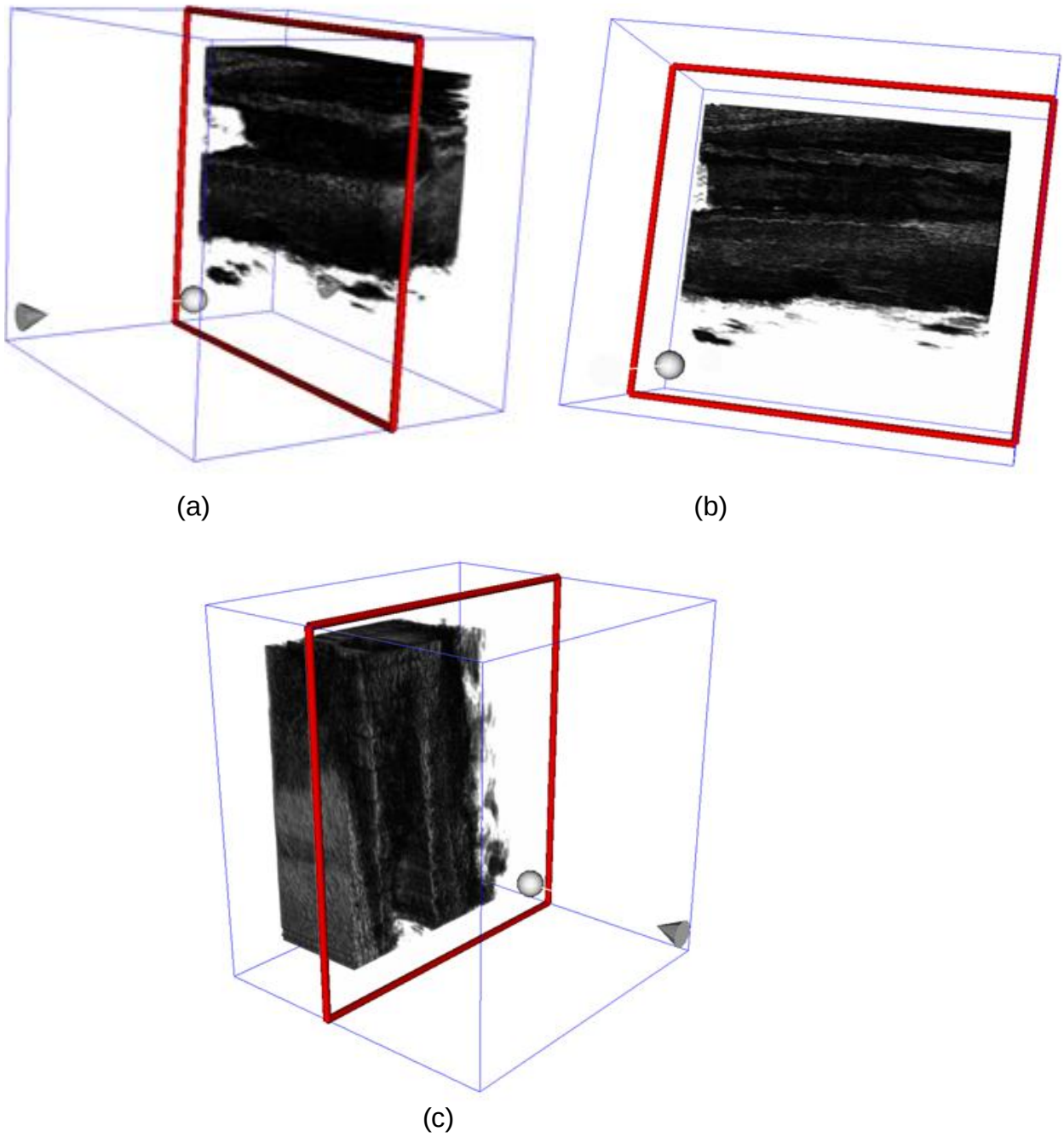


Figure 7. Internal view on interested subject carotid artery before 3D diffusion (a) front view (b) left side view, and (c) upper view.

rendering using our state-of-art algorithms. It is a real time free orientation 3D visualization in C++ platform on 2.4 GHz Pentium 4 processing unit.

Within appropriated algorithm's variables, the internal view of carotid arteries can be examined through virtual 3D slicers in any orientation, as shown in Figure 7. Similar to 2D ultrasound slices, it can be observed that the restructured 3D volume using un-processed 2D ultrasound slices comes with speckle noise. Besides, the internal structures of carotid arteries are also contaminated by the background cloud, which makes the challenging on precise measurement in small scale assessment. Fortunately, both difficulties are resolved by the proposed diffusion in 3D, as shown in Figure 8. We can observe that whole volume assembly was smoothed and the background clouds were eliminated. For example, Figure 9 shows the close views comparison sliced out from Figures 7b and 8b.

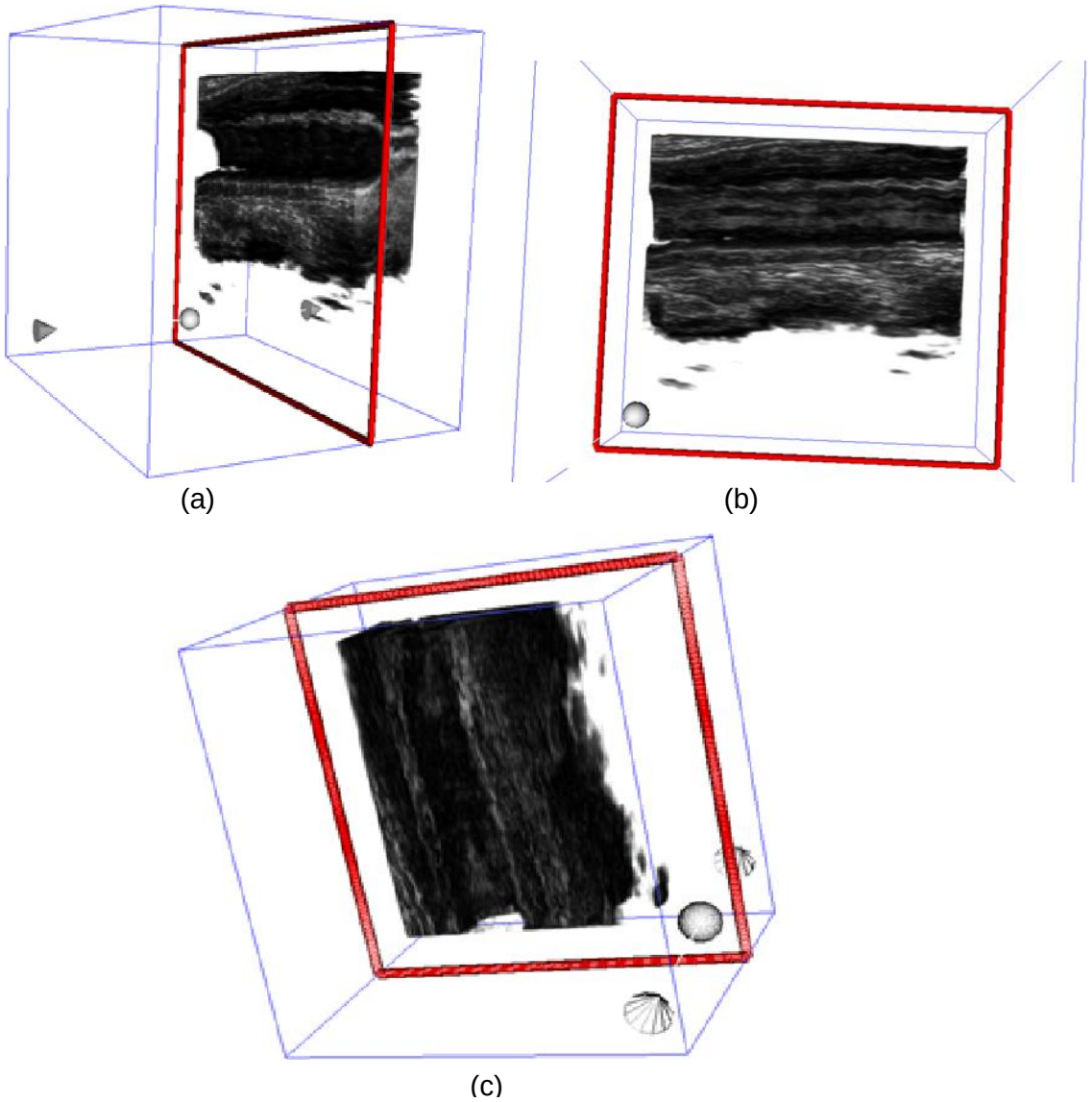


Figure 8. Internal view on interested subject carotid artery after 3D diffusion (a) front view (b) upper view, and (c) left side view.

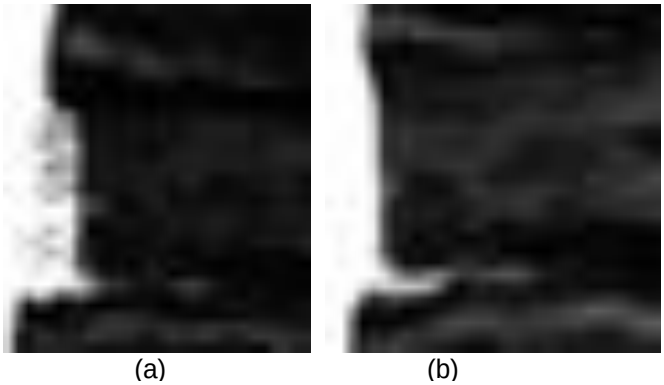


Figure 9. Comparison of simulation results (a) before diffusion, and (b) after diffusion.

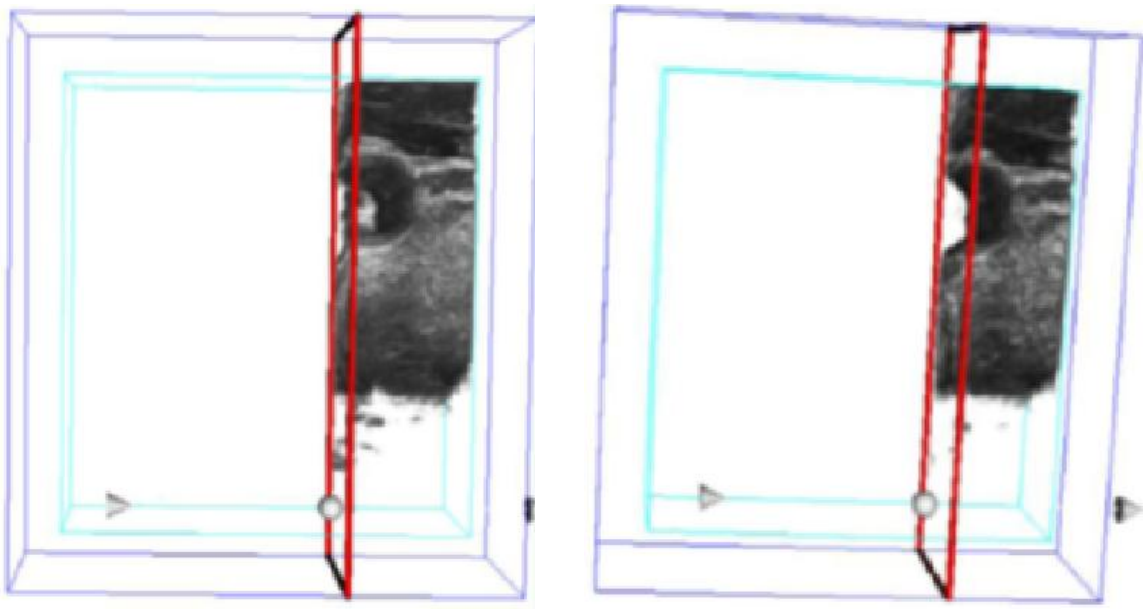


Figure 10. Background cloud-noise filtering effect (a) before 3D diffusion, and (b) after 3D diffusion.

To inspect the usefulness of proposed diffusion method in clear way, we have performed a detail comparison assessment on same 3D volume at the same position. Figure 10 shows the cloud-noises were eliminated effectively after 3D diffusion.

For quantitative analyzing, the root mean square error (RMSE), signal-to-noise ratio (SNR) and peak signal-to-noise ratio (PSNR) were utilized to prove the efficiency of the proposed method in restructured 3D ultrasound volumetric images. The tested images are sliced out from the restructured 3D ultrasound volumetric images in XZ plane.

RMSE calculates the average deviation from the original ultrasound image while SNR and PSNR are used to qualify how much an image has been affected by speckle noise. A quantitative measurement of the noise level is done by the image's standard deviation as shown in Equation 11.

$$\sigma = \sqrt{\frac{1}{N}\sum (b_i - b)^2} \quad , \text{i = 1, 2, 3…N} \quad (11)$$

where, *N* depicts the pixel number in the image, *b* depicts the original image's mean gray level and b_i depicts the surrounding region gray level value *e*. Mathematically, the statistical measurements can be indicated in the following equations where *f (i, j)* denotes original image and *F (i, j)* is image enhanced. For equation 14, the peak of grey value is set to 255, as the tested ultrasound images are 8 bit depth unsigned character.

$$RMSE = \sqrt{\frac{\sum (f(i,j) - F(i,j))^2}{MN}} \quad (12)$$

$$SNR = 10\log_{10} \frac{\sum_{i=1,\,j=1}^{M,N} (f(x,y))^2}{\sum_{i=1,\,j=1}^{M,N} (f(i,j) - F(i,j))^2} \quad (13)$$

$$PSNR = 20\log_{10} \frac{255}{RMSE} \quad (14)$$

Based on Table 2 RMSE of the proposed method is lower and the values SNR and PSNR are larger than SRAD. Larger RMSE represents a vast deviation from the original image which can affect the integrity as well as hurts the important information in ultrasound image. Meanwhile, PSNR and SNR reveal the highest value in the proposed method. This shows the enhancement of proposed method achieve a higher successfulness in speckle noise reduction on ultrasound image.

DISCUSSION

Since diffusion equation uses image gradient in monotonically decreasing function as diffusion coefficient, It will produce a larger diffusion coefficient in

Table 2. Statistical measurement.

Method	RMSE	SNR	PSNR
Proposed method	11.21	5.32	24.33
2D SRAD	27.04	4.32	19.17

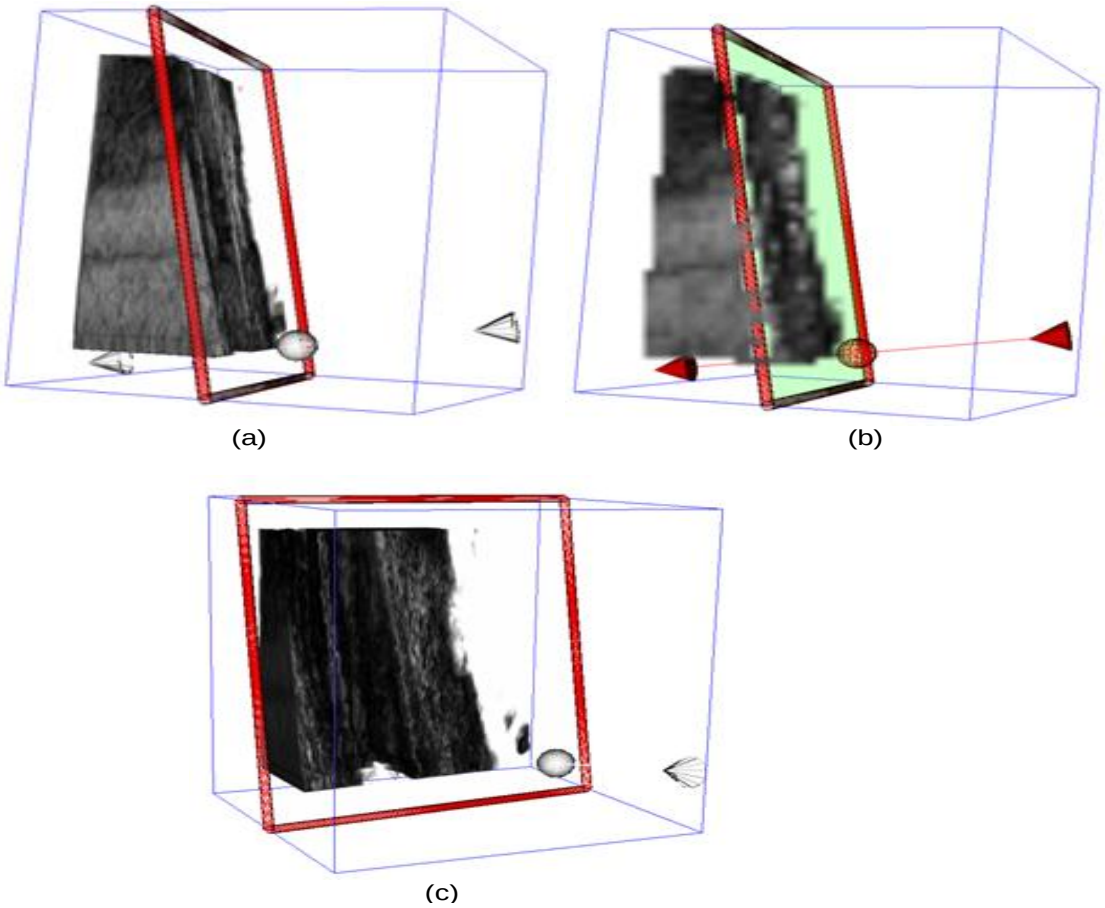


Figure 11. Simulation results with logjam phenomenon (a) before changing view position (b) rotation in progressed, and (c) rotation completed.

homogenous region with small gradient. Therefore, it can smooth the noise inside the homogenous regions effectively. Experimental results show that improved 2D SRAD is effective to remove speckle noise in 2D ultrasound images, and it is not dependent on window size selection in smoothing noise and image edge preservation. Yet, direct practice of existing 2D SRAD in 3D ultrasound volume rendering can cause external obstructive effect in Z-pixel direction, which further influence the morphology of the restructured 3D volume.

In actual computing, long execution time of partial differential equations is a disadvantage of 3D diffusion, where the image must be transformed into different iterative schemes. The large r number of iterations, a longer running time is necessary. Based on our findings, this condition will be further burdened when the 3D volume rendering consumes large buffered memories, while large numbers of 2D ultrasound slices were handled at the same time. This could cause computing logjam behavior during real time 3D position alignment as shown in Figure 11.

One way to improve the computing timing is using parallel computing technique. For image processing application in digitize form, it is possible to perform inter parallelism by duplicating several processing units in the system, where each of the processing unit is assigned to a segment frame. One other better proposed (Wenqian et al., 2006) solution is to integrate flexible FPGA

architecture to realize parallelism in computation. Multiple processing units are cascaded to process iterative algorithms in parallel, which could greatly reduce the computation time with speed-up ratio more than 20X.

Conclusion

Based on the foregoing analysis, diffusion on reconstructed three dimensional volume rendering should be taking consideration of voxel Z space for their topological and geometrical properties. These make the resultant 3D diffuse shape with better space coherence in every dimension. Findings shows the proposed 3D diffusion reflects better performance on volumetric ultrasound rendering compare to 2D anisotropic diffusion techniques.

ACKNOWLEDGEMENT

The researchers are so indebted and would like to express thaeir thankfulness to Prof. Dr. -Ing. habil. Jens Haueisen and Dr. rer. nat. Uwe Graichen for their support, comments and guidance throughout the project. We would also like to thank DAAD - Deutscher Akademischer Austausch Dienst for the financial support to the student who conducted the project at TU-Ilmenau, Germany. Our appreciation also goes to all the members of BMTI, Technische Universitat Ilmenau, Germany, for their ideas and support to the project.

REFERENCES

Catherine L, Tal A (2010). Measurement Selection in Untracked Freehand 3D Ultrasound. Medical Image Computing and Computer-Assisted Intervention. Lecture Notes in Computer Science, 6361: 127-134.

Christos PL, Constantinos SP (2011). Despeckle Filtering of Ultrasound Images. Atherosclerosis Dis. Manag., 2: 153-194.

Christos PL, Pattichis CS, Pantziaris M, Tyllis T, Nicolaides A (2006). Quality evaluation of ultrasound imaging in the carotid artery based on normalization and speckle reduction filtering. Med. Biol. Eng. Comput., 44(5): 414-426.

Czerwinski RN, Jones DL, O'Brien WD (1995). Ultrasound speckle reduction by directional median filtering. Proceeding of international conference on image processing, Washington, DC, USA, 1: 358-361.

Deepti M, Vinod K, Suresh CS, Niranjan K, Naveen K (2010). Enhancement of the ultrasound images by modified anisotropic diffusion method. Med. Biol. Eng. Comput., 48(12): 1281-1291.

Gerig G, Kubler O, Kikinis R, Jolesz FA (1992). Nonlinear anisotropic filtering of MRI data. IEEE Trans. Med. Imaging, 11(2): 221-232.

Gupta S, Chauhan RC, Saxena SC (2005). Robust non-homomorphic approach for speckle reduction in medical ultrasound images. Med. Biol. Eng. Comput., 43(2): 189-195.

Gupta S, Chauhan RC, Sexana SC (2003). Wavelet-based statistical approach for speckle reduction in medical ultrasound images. Med. Biol. Eng. Comput., 42(2): 189-192.

Kashif R, Nasir R, Noble JA (2008). Discrete Wavelet Diffusion for Image Denoising. Image and Signal Processing. Lecture Notes in Computer Science, 5099: 20-28.

Lee JS (1980). Digital image enhancement and noise filtering by using local statistics. IEEE Trans. Pattern Anal. Machine Intell., 2: 165-168.

Ling W, Deyu L, Tianfu W, Jiangli L, Yun P, Li R, Yi Z (2007). Filtering of medical ultrasonic images based on a modified anistropic diffusion equation. J. Elect., (China), 24(2): 209-213.

Min JK, Myoung HK (2007). Image Enhancing Technique for High-quality Visual Simulation of Fetal Ultrasound Volumes. Systems Mode. Simul., 2(16): 337-341.

Paula Z, Bernardino A, Homero S (2009). Comparison of Techniques for Speckle Noise Reduction in Breast Ultrasound Images. IFMBE Proceedings, World Congress on Medical Physics and Biomedical Engineering, Munich, Germany, 25(2): 569-571.

Perona P, Malik J (1990). Scale-space and edge detection using anisotropic diffusion. IEEE PAMI, 12(7):629-639.

Rajeev S, Gupta JRP (2010). A PDE-Based Nonlinear Filter Adapted to Rayleigh's Speckle Noise for De-speckling 2D Ultrasound Images. Contemporary Computing. Commun. Comput. Inform. Sci., 94(1): 1-12.

Shirzad S, Moghaddam HA, Alizadeh M (2009). Evaluation of wavelet-based methods for denoising ultrasonic echo signals. IFMBE Proceedings, World Congress on Medical Physics and Biomedical Engineering, Munich, Germany, 25(2): 666-669.

Wee LK, Chai HY, Eko S (2011a). Three dimensional nuchal translucency ultrasound segmentation using region growing for trisomy 21 early assessment. Int. J. Phys. Sci., 6(15): 3704-3710.

Wee LK, Hum YC, Eko S (2011b). Surface Rendering of Three Dimensional Ultrasound images using VTK. J. Sci, Industr. Res., 70: 421-426.

Wee LK, Hum YC, Supriyanto E (2011c). Computerized nuchal translucency three dimensional reconstruction, visualization and measurement for trisomy 21 prenatal early assessment, Int. J. Phys. Sci., 6(19): 4640-4648.

Wee LK, Min TY, Arooj A, Eko S (2010). Nuchal Translucency Marker Detection Based on Artificial Neural Network and Measurement via Bidirectional Iteration Forward Propagation. WSEAS Trans. Inform. Sci. Appl., 8(7): 1025-1036.

Wee LK, Supriyanto E (2010). Computerized Automatic Nasal Bone Detection based on Ultrasound Fetal Images Using Cross Correlation Techniques. WSEAS Trans. Inform. Sci. Appl., 8(7): 1068-1077.

Wenqian Wu, Scott T. Acton, John Lach (2006). Real-Time Processing of Ultrasound Images with Speckle Reducing Anisotropic Diffusion, Fortieth Asilomar Conference on Signals, Systems and Computers, Pacific Grove, CA, 1458-1464.

Yu BU Lee, Min-Jeong Kim, Myoung-Hee Kim (2007). Robust border enhancement and detection for measurement of fetal nuchal translucency in ultrasound images. Med. Biol. Eng. Comput., 45(11): 1143-1152.

Yu Y, Acton S (2002). Speckle reducing anisotropic diffusion. IEEE Trans Image Process. 11(11): 1260-1270.